INCREASING THE EFFICIENCY OF MULTICRYSTALLINE SILICON PERC SOLAR CELLS FROM CURRENTLY 19% TO 20%

J.M. Greulich, E. Lohmüller, P. Saint-Cast, S. Werner, S. Wasmer, A.J.C. van der Horst, R. Preu
Fraunhofer Institute for Solar Energy Systems
Heidenhofstr. 2, 79110 Freiburg, Germany

ABSTRACT: We discuss a detailed analysis of the potential efficiency improvements of state-of-the-art industrial p-type multicrystalline silicon solar cells with passivated emitter and rear with an average energy conversion efficiency of 19.0%. The aim is to identify the limitations of cells currently fabricated in industry, not of record laboratory cells, and to demonstrate approaches for research institutes and industry to further optimise the devices using industrially applicable processes. According to the analysis, front surface reflection of the active cell area bears the largest potential for increasing the efficiency by replacing the standard acidic texture by a honeycomb texture, which is estimated to improve the efficiency from 19% to 20%. Reducing shading and recombination at the front metal is the second largest potential efficiency increase. We expect that reducing the metal finger width from 50 μm to 40 μm or below is feasible and increases the efficiency further to 20.2%.

Keywords: multicrystalline silicon, characterisation, optical losses, recombination, simulation

1 INTRODUCTION

Passivated emitter and rear solar cells (PERC) [1] based on p-type multicrystalline silicon (mc-Si) are relevant for industry and research for two main reasons: First, mc-Si is the workhorse of photovoltaics with a market share of more than 60% [2] and is expected to keep cost-competitive as simple solutions for texturing diamond-wire cut mc-Si wafers are available [3, 4]. Second, PERC technology is being introduced into mass production in the past few years and is rapidly gaining market share also due to the recent record cell [5, 6] and module efficiencies [7]. To stay cost-competitive, research and industry aim at increasing the energy conversion efficiency without increasing the manufacturing costs. The key to improve the solar cell efficiencies is to know of the bottlenecks of the solar cells in terms of lost power in its different regions.

The free energy loss analysis introduced by Brendel *et al.* [8] and extended to optical losses by Greulich *et al.* [9] quantifies the power losses at each mesh node of the numerical simulations due to electrical and optical effects, while integrating over certain device regions yields their contribution to the total power losses. These losses are directly comparable. However, elaborate numerical device simulations are needed.

Aberle *et al.* [10] published a method which compares the single, experimentally determined loss mechanisms in units of mW/cm², but only took into account the overall recombination occurring in the solar cell and does not differentiate the contributions by the different solar cell regions.

The experimental loss analysis conducted by Wong *et al.* [11] and Saint-Cast *et al.* [12] divides the examinations into a breakdown of the loss mechanisms impacting the short-circuit current density j_{sc}, the open-circuit voltage V_{oc} and the fill factor FF. This has the drawback that the single losses cannot be compared, as the performance parameters j_{sc}, V_{oc} and FF are investigated separately.

Further approaches for optimising the efficiency [13, 14] allow very deep insights into the physics of the device, but require elaborate numerical device simulations and do not directly rely on measured data.

In the present work, we characterise and disclose the losses and potential efficiency improvements of state-of-the-art industrial p-type mc-Si PERC cells. An advanced analysis that does not only derive the losses and potential improvements for maximum power point (mpp) conditions from measurements at short and open circuit, but directly measures recombination currents at mpp is applied. Besides analysing the losses, also the realistic efficiency potential is examined using PC1Dmod [15] simulations.

2 THEORY

The basis of the advanced efficiency potential analysis is formed by three components: (i) optical losses, (ii) recombination losses and (iii) transport losses. It is based on measured data and includes only analytical calculations. All losses are expressed as power density. The details of the approach are discussed in Ref. [16], here only the basics are summarised.

The optical losses comprise reflection by the front metal grid, reflection by the active cell area, escape light and parasitically absorbed light. For their quantification, the external quantum efficiency (EQE) and the spectral reflectance (R) are measured. By weighting with the photon flux of the AM1.5g spectrum, the internal quantum efficiency at maximum power point, the loss currents $j_{opt,x}$ corresponding to the individual losses "x" (e.g. reflectance at front metal or active cell area) are determined. By multiplying this quantity with the voltage V_{mpp} at maximum power point, the corresponding power loss or potential power gain is calculated.

The recombination losses comprise recombination in the emitter, in the base, at the rear surface and at the front and rear metal-semiconductor contacts. Corresponding lifetime samples (samples to determine the emitter dark saturation current density j_{0e}; samples to determine the implied V_{oc} (iV_{oc}) with and without front / rear metal contacts) are required and are characterised by means of photoluminescence calibrated to the (implied) V_{oc}. The excitation conditions are carefully chosen to ensure similar injection conditions in the lifetime samples as in the finished solar cells at mpp (i.e., the laser intensity is tuned to generate an implied voltage of the lifetime samples equal to the junction voltage at mpp). From these measurements, the recombination current at mpp, corresponding to the above losses, is derived. Again, by multiplying this quantity with the voltage V_{mpp} at mpp,

the corresponding power loss or potential power gain is calculated.

Finally, we consider losses due to series resistance as follows. From each of the single, measurable resistances of emitter sheet resistance R_{sh}, front contact resistivity ρ_C, front grid resistance R_{grid} and rear aluminium resistance R_{Al}, we calculate the single contributions $R_{s,x}$ to the total series resistance R_s via analytical formulae. As we want to rely on measurements and analytical modelling only, we estimate the base resistance by subtracting the sum of the aforementioned contributions from the total R_s of the solar cells. In order to obtain loss power densities, the single series resistance contributions $R_{s,x}$ are simply multiplied by the squared current density flowing at mpp j_{mpp}.

This approach gives a rough orientation to identify which losses are dominant and shall be improved first, and which can be neglected to first order.

The efficiency potential of selected process improvements, i.e., an advanced front surface texture and an improved front metal grid, is estimated by applying measured data to a PC1Dmod [15] simulation model.

3 EXPERIMENTAL

Solar cells and lifetime samples are fabricated in the PV-TEC pilot line [17] at Fraunhofer ISE. Industrial tools are used for each of the solar cell fabrication processes. A group of six cells, which is part of a larger experiment, is analysed here.

The solar cell fabrication process is presented in Figure 1. Regular sized wafers with an edge length of 156 mm are used. The p-type base material is high-performance mc-Si with a base resistivity ranging between 1.4 Ωcm and 1.8 Ωcm. After saw-damage removal, the wafers undergo acidic texturing using hydrofluoric (HF) and nitric acid (HNO$_3$). The emitter is formed by phosphorus diffusion in a tube furnace utilizing phosphorus oxychloride (POCl$_3$). After diffusion, the emitter is removed at the rear using a single-sided wet-chemical etching process. Prior to passivation, the samples are cleaned using HF and HNO$_3$. The passivation layer stack on the rear surface is formed by fast atomic layer deposition of aluminium oxide (Al$_2$O$_3$) covered by a silicon nitride (SiN$_x$) capping using plasma-end chemical vapour deposition (PECVD). The front surface is passivated by a PECVD SiN$_y$ layer. A double-layer antireflection coating (ARC) is also applied on a separate group. The rear passivation is opened using
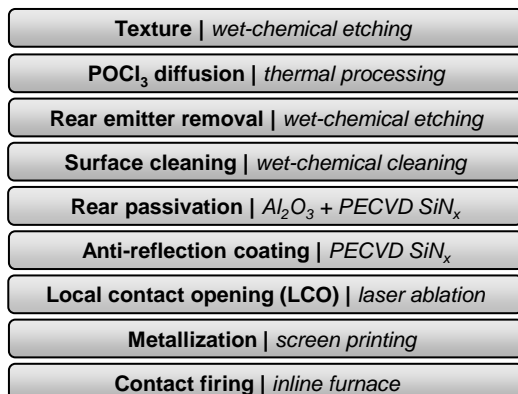
Figure 1: Process flow for the fabrication of p-type mc-Si PERC solar cells applied in this work.
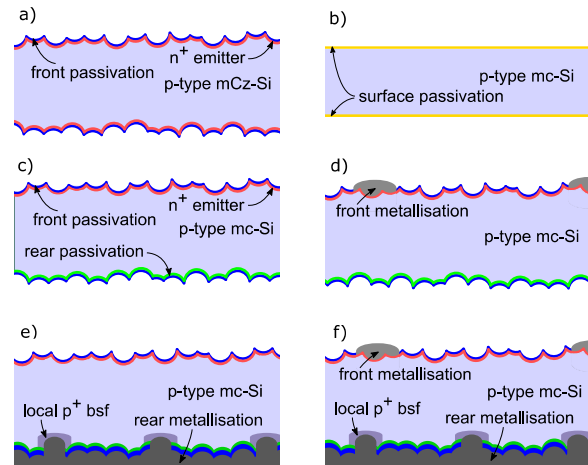
Figure 2: a) The symmetric j_{0e}-samples are based on monocrystalline p-type mCz-Si wafers with acidic texture, emitter and SiN$_y$ passivation. b) The bulk-lifetime (τ_b) samples consist of etched-back iV_{oc}-samples with a smoothened surface passivated with PECVD Al$_2$O$_3$. c) The iV_{oc}-samples are based on mc-Si, have the same front as the j_{0e}-samples, but the rear is passivated with Al$_2$O$_3$ and SiN$_x$. d) iV_{oc}-samples including front metallisation. e) iV_{oc}-samples including rear local contact opening and rear metallisation. f) Finished solar cells. All samples are fired in a conveyor belt oven prior to characterisation.

a laser ablation process. The front and rear metallisation are obtained by screen printing, where a five busbar design is applied. The finger width after firing is $w_f \approx 50$ µm. After contact firing, the solar cells are characterised.

The cross sections of the lifetime samples and the cells are sketched in Figure 2. The emitter dark saturation current density $j_{0e} \approx 80$ fA/cm² is measured on symmetrical lifetime samples (Figure 2a) based on monocrystalline p-type mCz-Si wafers applying a refinement of the Kane-Swanson method [18]. The iV_{oc} of the corresponding lifetime samples in Figure 2c is determined using lifetime-calibrated photoluminescence imaging (τ-PLI). Its value is determined to $iV_{oc} = 665$ mV with a standard deviation within each sample of approximately 10 mV.

The current-voltage (*IV*) characteristics, the external quantum efficiency (EQE) and the spectral reflectance R of the cells are measured. The cells have a mean $j_{sc} = 37.1$ mA/cm², a $V_{oc} = 649$ mV and an average conversion efficiency $\eta = 19.0\%$. The peak efficiency of this batch is 19.4%, which is confirmed by Fraunhofer ISE CalLab PV Cells. When applying a double-layer anti-reflection coating, an efficiency of 19.6% is independently measured by Fraunhofer ISE CalLab PV Cells.

4 RESULTS

We find that first optical, then recombination and finally resistive losses or potential efficiency improvements play subsequent roles in the overall analysis, as shown in Figure 3. Above all, reducing the reflection at the active front side could improve the efficiency by 1.6%$_{abs}$, e.g. by replacing the common
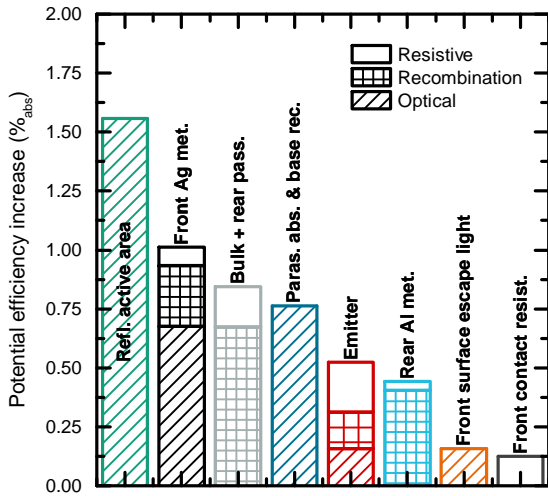
Figure 3: Potential efficiency improvements subdivided in optical, recombination and resistive contributions for different cell regions.

acidic iso-texturing process used for mc-Si wafers. Furthermore, the mc-Si cell should then be optimized concerning the bulk material quality with a potential efficiency gain of $0.7\%_{abs}$, as here the recombination at the front side plays only a minor role ($0.4\%_{abs}$). For "Paras. abs. & base rec.", PC1Dmod simulations showed that most is due to parasitic absorption and mainly occurring at the rear side in the aluminium metallization. Therefore, $0.8\%_{abs}$ could be gained next by mitigating the parasitic absorption, as. Technologically, this could be addressed by optimizing the rear side passivation stack for optical ends [19]. The potential efficiency gains due to resistive influences are not dominant as these sum up to only $0.6\%_{abs.}$

This analysis shows the potential efficiency improvements of individual loss mechanisms if that loss mechanism could be reduced to zero. A more realistic estimation of the potential efficiency is done using a PC1Dmod simulation model. First, it is calibrated using the measured data (reflectance, EQE, *IV* data). The above analysis suggests to first focus on reducing the front reflection. Hence, the first optimisation step is an advanced surface texture, *i.e.* a honeycomb texture. Integrating this process will reduce the reflection and potentially increase the recombination at the emitter as shown by Volk *et al.*in Ref. [20]. We use the measured reflectance of honeycomb textured test samples with anti-reflection coating as input of the modified PC1Dmod model. Thus, the weighted reflectance of the active area

Table I: Important input and output of the PC1Dmod simulation model for the experimentally realised baseline and the two simulated optimisation scenarios.

	baseline	improved texture	improved grid
R_{wa} [%]	6.8	2.3	2.3
$j_{0e,eff}$ [fA/cm²]	100	130	125
w_f [μm]	50	50	40
$R_{s,ext}$ [Ωcm²]	0.39	0.39	0.41
j_{sc} [mA/cm²]	37.2	39.2	39.5
V_{oc} [mV]	646.0	645.6	645.8
η [%]	19.0	20.0	20.2

R_{wa} is decreased, and the effective emitter saturation current density $j_{0e,eff}$, which contains contributions of the metallised and the passivated emitter, is increased by applying an advanced front surface texture (see Table I). The simulation then predicts an efficiency increase from 19.0% to 20.0%. In an additional second optimisation step, the front grid finger width w_f is reduced by assuming an advanced screen-printing process, which also slightly reduces the recombination at the metal-emitter interface, which is reflected in the PC1Dmod model by a lower $j_{0e,eff}$. Improving the front metal shading by reducing the finger width from 50 μm to 40 μm would decrease the shading losses and recombination at the metal-emitter interface, but it would also slightly increase the series resistance. This results in a simulated efficiency of 20.2%.

5 SUMMARY AND CONCLUSIONS

In this work, we applied a method to conduct a thorough efficiency gain analysis to 19%-efficient p-type multicrystalline silicon (mc-Si) PERC solar cells fabricated in an industrial manner. The method relies exclusively on experimental input without the need of simulations. For that end, we determined the contribution of every loss mechanism under maximum power point conditions of the solar cell.

The gain analysis revealed that the reflectance of the active front side area bears the largest potential for optimisation, and the front metallisation the second largest potential. Based on these findings, we conducted PC1Dmod simulations to estimate the achievable efficiency under realistic assumptions. When applying a honeycomb texture, the efficiency is predicted to increase to 20.0%. Reducing the front grid finger width from currently 50 μm to 40 μm is estimated to further increase the efficiency to 20.2%.

The present work presents a systematic method for research institutes to guide research activities and allows cell manufacturers to identify, understand and minimise losses of their cells by comparing their internal results with ours. These results can be used to steer future research activities.

6 ACKNOWLEDGMENT

7 REFERENCES

[1] A. W. Blakers, A. Wang, A. M. Milne, J. Zhao, and M. A. Green, "22.8% efficient silicon solar cell," *Appl. Phys. Lett.*, vol. 55, no. 13, pp. 1363–1365, 1989.

[2] ITRPV, "International Technology Roadmap for Photovoltaic: 2016 Results," 2017. [Online] Available: http://www.itrpv.net/Reports/Downloads/.

[3] SCHMID Group | Gebr. SCHMID GmbH, *SCHMID develops new process for the texturing of diamond-wire-cut multi-wafers: Press release, Feb 2, 2017.*

[4]   RENA Technologies GmbH, *Advanced texturing solutions and large orders from major Asian customers.* [Online] Available: https://www.rena.com/de/unternehmen/news/news/ advanced-texturing-solutions-and-large-orders-from-major-asian-customers/. Accessed on: Aug. 31 2017.

[5]   Trina Solar, *Trina Solar Announces New Efficiency Record of 21.25% Efficiency for Multi-crystalline Silicon Solar Cell: Press release, Nov 09, 2015.*

[6]   Fraunhofer Institute for Solar Energy Systems (ISE), *Multicrystalline Silicon Solar Cell with 21.9 Percent Efficiency: Fraunhofer ISE Again Holds World Record,* 2017.

[7]   Hanwha Q CELLS, *HANWHA Q CELLS Achieves New World Record in Multicrystalline Solar Module Efficiency: Press release, Jun 20, 2016.*

[8]   R. Brendel, S. Dreissigacker, N.-P. Harder, and P. P. Altermatt, "Theory of analyzing free energy losses in solar cells," *Appl. Phys. Lett.*, vol. 93, no. 17, p. 173503, 2008.

[9]   J. Greulich, H. Höffler, U. Würfel, and S. Rein, "Numerical power balance and free energy loss analysis for solar cells including optical, thermodynamic, and electrical aspects," *J. Appl. Phys.*, vol. 114, no. 20, p. 204504, 2013.

[10]   A. G. Aberle, W. Zhang, and B. Hoex, "Advanced loss analysis method for silicon wafer solar cells," *Energy Procedia*, vol. 8, pp. 244–249, 2011.

[11]   J. Wong, S. Duttagupta, R. Stangl, B. Hoex, and A. G. Aberle, "A Systematic Loss Analysis Method for Rear-Passivated Silicon Solar Cells," *IEEE J. Photovoltaics*, vol. 5, no. 2, pp. 619–626, 2015.

[12]   P. Saint-Cast *et al.,* "Analysis of the losses of industrial-type PERC solar cells," *Phys. Status Solidi A*, vol. 214, no. 3, p. 1600708, 2017.

[13]   B. Min *et al.,* "Incremental efficiency improvements of mass-produced PERC cells up to 24%, predicted solely with continuous development of existing technologies and wafer materials," in *31st EU PVSEC*, Hamburg, Germany, 2015, pp. 473–476.

[14]   Sven Wasmer, Andreas A. Brand, Johannes M. Greulich, "Metamodeling of numerical device simulations to rapidly create efficiency optimization roadmaps of monocrystalline silicon PERC cells," in *7th International Conference on Silicon Photovoltaics*.

[15]   H. Haug and J. Greulich, "PC1Dmod 6.2 – Improved Simulation of c-Si Devices with Updates on Device Physics and User Interface," *Energy Procedia*, vol. 92, pp. 60–68, 2016.

[16]   Sven Wasmer, Abraham van der Horst, Pierre Saint-Cast, Johannes Greulich, "Experimental Efficiency Gain Analysis of Passivated Emitter and Rear Silicon Solar Cells, to be published," *IEEE J. Photovoltaics*, 2017.

[17]   D. Biro *et al.,* "PV-TEC: Retrospection to the three years of operation of a production oriented research platform," in *24th EU PVSEC*, Hamburg, 2009, pp. 1901–1905.

[18]   A. Kimmerle, J. Greulich, and A. Wolf, "Carrier-diffusion corrected J0-analysis of charge carrier lifetime measurements for increased consistency," *Sol. Energy Mater. Sol. Cells*, vol. 142, pp. 116–122, 2015.

[19]   Z. C. Holman *et al.,* "Parasitic absorption in the rear reflector of a silicon solar cell: Simulation and measurement of the sub-bandgap reflectance for common dielectric/metal reflectors," *Solar Energy Materials and Solar Cells*, vol. 120, pp. 426–430, 2014.

[20]   A. Volk *et al.,* "Honeycomb structure on multi-crystalline silicon Al-BSF solar cell with 17.8% efficiency," *IEEE Journal of Photovoltaics*, vol. 5, no. 4, pp. 1027–1033, 2015.